




## Article

# Mini-LEDs with Diffuse Reflection Cavity Arrays and Quantum Dot Film for Thin, Large-Area, High-Luminance Flat Light Source

Zhi Ting Ye <sup>1,\*</sup> , Yuan Heng Cheng <sup>1</sup>, Ku Huan Liu <sup>2</sup> and Kai Shiang Yang <sup>2</sup>

<sup>1</sup> Department of Mechanical Engineering, Advanced Institute of Manufacturing with High-Tech Innovations, National Chung Cheng University, No. 168 University Road, Minxiong Township, Chiayi County 621301, Taiwan; g09421023@ccu.edu.tw

<sup>2</sup> EPOCH CHEMTRONICS Corp, Hsinchu County 302006, Taiwan; GuuhuannLiu@epoch-optic.com (K.H.L.); t102568060@ntut.org.tw (K.S.Y.)

\* Correspondence: imezty@ccu.edu.tw

**Abstract:** Mini-light-emitting diodes (mini-LEDs) were combined with multiple three-dimensional (3D) diffuse reflection cavity arrays (DRCAs) to produce thin, large-area, high-brightness, flat light source modules. The curvature of the 3D free-form DRCA was optimized to control its light path; this increased the distance between light sources and reduced the number of light sources used. Experiments with a 12.3-inch prototype indicated that 216 mini-LEDs were required for a 6 mm optical mixing distance to achieve a thin, large-area surface with high brightness, uniformity, and color saturation of 23,044 cd/m<sup>2</sup>, 90.13%, and 119.2, respectively. This module can serve as the local dimming backlight in next generation automotive displays.

**Keywords:** mini-light-emitting diode; uniformity; luminance; diffuse reflection cavity array; quantum dot film



**Citation:** Ye, Z.T.; Cheng, Y.H.; Liu, K.H.; Yang, K.S. Mini-LEDs with Diffuse Reflection Cavity Arrays and Quantum Dot Film for Thin, Large-Area, High-Luminance Flat Light Source. *Nanomaterials* **2021**, *11*, 2395. <https://doi.org/10.3390/nano11092395>

Academic Editors: Iván Mora-Seró and Jong-Soo Lee

Received: 29 July 2021

Accepted: 13 September 2021

Published: 14 September 2021

**Publisher's Note:** MDPI stays neutral with regard to jurisdictional claims in published maps and institutional affiliations.



**Copyright:** © 2021 by the authors. Licensee MDPI, Basel, Switzerland. This article is an open access article distributed under the terms and conditions of the Creative Commons Attribution (CC BY) license (<https://creativecommons.org/licenses/by/4.0/>).

## 1. Introduction

Display technology has developed rapidly, starting in the second half of the 20th century, and various types of displays have become ubiquitous in daily life. For example, light-emitting diodes (LEDs) have replaced conventional cathode-ray tubes. LEDs afford advantages such as higher color performance, low energy consumption, and eco-friendliness, and therefore, they are the principal backlight source of liquid crystal displays (LCDs) [1–4]. However, because of the demand for high resolution, high color saturation, and pixel quality, technologies including organic LEDs (OLEDs), mini-LEDs, micro-LEDs, quantum dot LEDs (QD-LEDs), laser displays, and holographic displays have been developed to replace LCDs. Nevertheless, LCDs remain the standard in the market and are widely used in smartphones, tablet computers, televisions, and other display devices [5–8]. As mentioned, LED light sources are used as LCD backlight sources. According to the position of the light source, they are divided into direct-type and side-type backlight modules. Direct-type backlights have lower cost, higher optical efficiency, and straightforward design compared with side-type backlights, and therefore, they have become dominant in the large-sized LCD backlight module market [9–11]. Although LCDs feature advantages such as low power consumption, long service life, and low cost, their slow response time, low color saturation, and low photoelectric conversion efficiency (typically <10%) are currently their main drawbacks [12–15]. To improve color saturation, color conversion materials with high response speed and high color saturation can be used. Furthermore, RGB chips can be used to form a white light source to increase the display color gamut. However, because of the relatively low efficiency of red LED chips, increasing the current and output power shortens the life of the chip. Blue LEDs with a GaN base and the green

phosphor  $\beta$ -SiAlON and red phosphor  $K_2SiF_6$  are commonly used as a high color gamut space backlight [16–18].

Quantum dots (QDs) are a new color conversion material that have a narrower full width at half-maximum (FWHM); therefore, they have a wider color gamut and higher quantum efficiency. As a result, novel QD-LEDs are gradually being applied to LCD backlight modules [19–22]. In addition, there are many studies that provide related synthesis protocols of quantum dots [23,24].

The strong demand for high-end displays such as gaming monitors, car monitors, and notebook computers has driven an increased demand for high dynamic area contrast backlights (i.e., high dynamic range [HDR]). Conventional LCD edge-lit backlights are only distributed on the light guide plate. Whether single- or double-sided, this architecture allows limited contrast control. Mini-LEDs, because of their smaller size and high current density injection drive, can achieve high-contrast HDR and high brightness. Mini-LEDs are thus considered a promising backlight source for next-generation high-end LCDs [25–27].

Mini-LEDs have a smaller package size than conventional LEDs. The light-emitting angle is limited to approximately  $120^\circ$ ; therefore, more LEDs are required to achieve a uniform surface light source. Furthermore, the light line is not adjusted for HDR backlights, resulting in a halo. This problem causes the contrast to decrease, and the smaller area of the light source body causes the problem of heat source concentration [28–31].

Although the thickness of the backlight module can be reduced and the uniformity can be improved by increasing the number of mini-LEDs, this method is not the preferred design. Researchers have optimized the light output angle to reduce the total number of particles in the light source by adjusting the optical design [32,33]. For example, Ye et al. proposed a hollow tube structure containing mini-LEDs with asymmetrical luminous intensity and designed a beveled reflective surface on the side of the mini-LEDs to achieve high efficiency and high uniformity. Moreover, they proposed a flat light source module without a light guide plate with a dot pattern and a completely printed diffuse reflection light guide plate on the bottom surface of the light source module to achieve high efficiency and high uniformity [34,35]. Ohno proposed an LED lighting module with a coaxial light conductor to achieve high efficiency and high wide-angle performance [36]. Lu et al. proposed a transparent array of mini-LEDs on a polyethylene terephthalate (PET) substrate. They found that, at room temperature, the mini-LEDs exhibited high uniformity and wideness and stable color gamut performance. Lin et al. proposed a direct-illuminated LED free-form lens array with a Cartesian candela distribution. Through the incorporation of free lenses and diffusers, the LED lens array was optimized to improve uniformity. Zhu et al. proposed a free-form surface design method for LEDs to achieve diffusion and transmission. This lighting system affords advantages such as high efficiency and high uniformity [37–39].

Huang et al. proposed a chip-level package with a free-form package design that has ultrahigh light extraction efficiency and a batwing-shaped light field to provide a thin, high-wide-angle and low-profile package for reducing the number of LEDs. Li et al. proposed a two-layer encapsulation structure that combines  $SiO_2$  and graphite nanoparticles to improve the uniformity and environmental contrast. Chen et al. proposed a direct lighting mini-chip-level packaged LED that combines a QD film with a diffuser and prism films to improve the brightness and uniformity and to reduce the number of LEDs used [40–42].

Park et al. proposed a flip-chip package and a vertical chip package structure for InGaN/GaN stripe LEDs to achieve higher uniformity and to improve the light extraction efficiency. Tang et al. proposed the use of tetramethylammonium hydroxide to construct a layered structure on the sidewall of mini-LEDs by anisotropic etching to improve the light extraction efficiency of the mini-LEDs [43,44].

Zhu et al. proposed double freeform surface lens with diffuse reflection applied in non-imaging optical systems [45]. Zhu et al. proposed diffuse reflective Off-Axis surface for noncircular LED arrays [46]. Although these two designs can achieve large-area light sources, they cannot achieve a thin, high-luminance, flat light source. Sho et al. proposed a

thin mini-LEDs backlight using reflective mirror dots to obtain high luminance uniformity for mobile LCDs [47].

In summary, related studies have attempted to improve the light output efficiency, uniformity, and color saturation of planar light sources. However, the use of large-area planar light sources to reduce the number of LEDs used requires further study.

This study proposes mini-LEDs combined with multiple three-dimensional (3D) diffuse reflection cavity arrays (DRCAs) to achieve a thin, large-area, and high-luminance planar light source.

## 2. Materials and Method

### 2.1. Simulation of Optical Module and Light Film Material Selection for Mini-LEDs

Soliwork3D drawing software and Light Tools optical simulation software were used to construct the optical system and optimize the diffuse reflection cavity module. The optical components include multiple 3D DRCAs, diffusers, QD films, and a brightness enhancement film (BEF). The influence of brightness and uniformity was analyzed. Figure 1 presents a schematic of the structure of the mini-LEDs combined with the 3D DRCA.

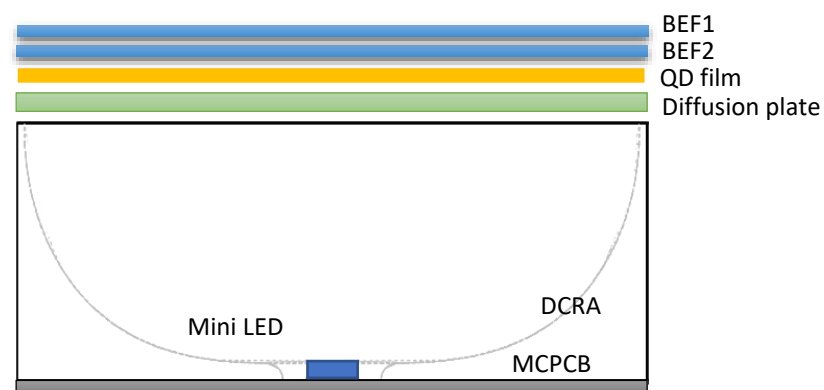


Figure 1. Schematic of the structure of mini-LEDs combined with 3D DRCA.

The light source uses Epistar YR-CV1010BDAN mini-LEDs. The package length  $L_{PKG}$ , package width  $W_{PKG}$ , package height  $H_{PKG}$ , chip PAD length  $L_{PAD}$ , and chip PAD width  $W_{PAD}$  are 1 mm, 1 mm, 0.4 mm, 0.903 mm, and 0.328 mm, respectively, and Figure 2 displays the package size of the mini-LEDs.

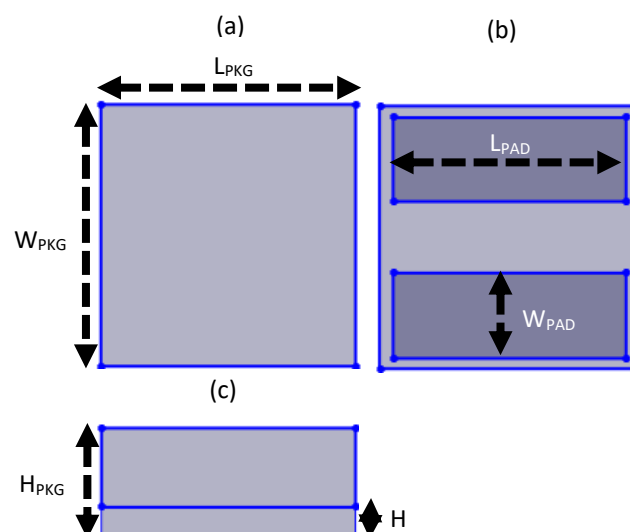


Figure 2. Structure of mini-LEDs. (a) top view, (b) bottom view, and (c) side view.

Figure 3 illustrates the light distribution curve of the mini-LEDs. The half-intensity angle FWHM is 160°, and the 0° angle intensity at the center is approximately 90%.

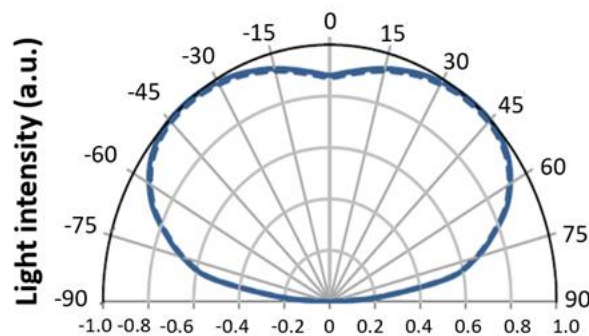


Figure 3. Mini-LED chip light distribution curve.

### 2.2. Model Construction of DRCA

A Bezier curve (B) was used to analyze the optimal curvature for the DRCA, as given by Equation (1).

$$B(t) = (1 - t)^3 P_a + 3(1 - t)^2 t P_b + 3(1 - t) t^2 P_c + t^3 P_d, t \in [0, 1] \tag{1}$$

where the four points  $P_a, P_b, P_c,$  and  $P_d$  define a cubic Bezier curve in a plane or in a 3D space. The curve goes from  $P_a$  to  $P_b$  in the direction from  $P_c$  to  $P_d$ . Generally, it does not pass through  $P_b$  or  $P_c$ ; these two points provide direction information. The distance between  $P_a$  and  $P_b$  determines the length of the curve in the direction of  $P_b$  before turning to  $P_c$ .

The equation of the Bezier curve is a continuous function; therefore, its derivative is obtained as follows:

$$B'(t) = 3tC_1 + 2tC_2 + C_3 \tag{2}$$

$C_1, C_2,$  and  $C_3$  are coefficients that are given as follows:

$$C_1 = (-P_a + 3P_b - 3P_c + P_d), C_2 = (3P_a - 6P_b + 3P_c), \text{ and } C_3 = (-3P_a + 3P_b) = P_a \tag{3}$$

The light field shape of the mini-LEDs was used to simulate the diffuse reflection cavity, and the light was evenly distributed to the diffuser through an optimized design, thereby evenly expanding the projection area of the light source. Figure 4 presents a schematic of the light trace.

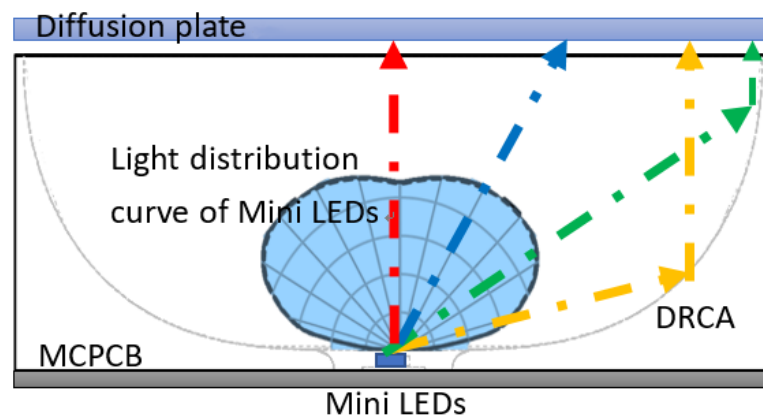


Figure 4. Schematic of diffuse reflection cavity light trace.

The parameters of the diffuse reflection cavity were set to the Lambertian diffuse surface characteristics: the diffuse reflectance was 94%, QD film was set to the Lambertian diffuse transmittance of 50%, reflectance was 50%, refractive index of the BEF was 1.56, and

apex angle was  $90^\circ$ . The surface of the metal core printed circuit board (MCPCB) was set to the Lambertian diffuse surface reflectance of 90%, center wavelength of the light source was 450 nm, input power was normalized as 1 W, and number of rays was 50 million for simulation. Table 1 lists the parameter settings.

**Table 1.** Simulation parameter settings.

BEF1	The refractive index = 1.56, the apex angle = 90 degrees
BEF2	The refractive index = 1.56, the apex angle = 90 degrees
diffuse reflection cavity array, DRCA	Lambertian diffusion surface characteristics, Reflectance 94%
QD film	Lambertian diffusion surface characteristics, 50% transmittance and 50% reflectivity
MCPCB	Lambertian diffusion surface characteristics, Reflectance 90%
Light source	Input light 1 W Center wavelength 450 nm 50 million rays

$L_{DRCA}$ ,  $W_{DRCA}$ , and  $H_{DRCA}$  of the simulated diffuse reflection cavity matrix module were 48.8, 48.72, and 4.57 mm, respectively. Furthermore, the mini-LED spacing mini-LEDs<sub>p</sub> was 12 mm, optical mixing distance between the mini-LEDs and the diffuser was 6 mm, and the simulation of the design optimization was based on a  $4 \times 4$  diffuse reflection cavity matrix. Figure 5 illustrates the 3D structure of the module.

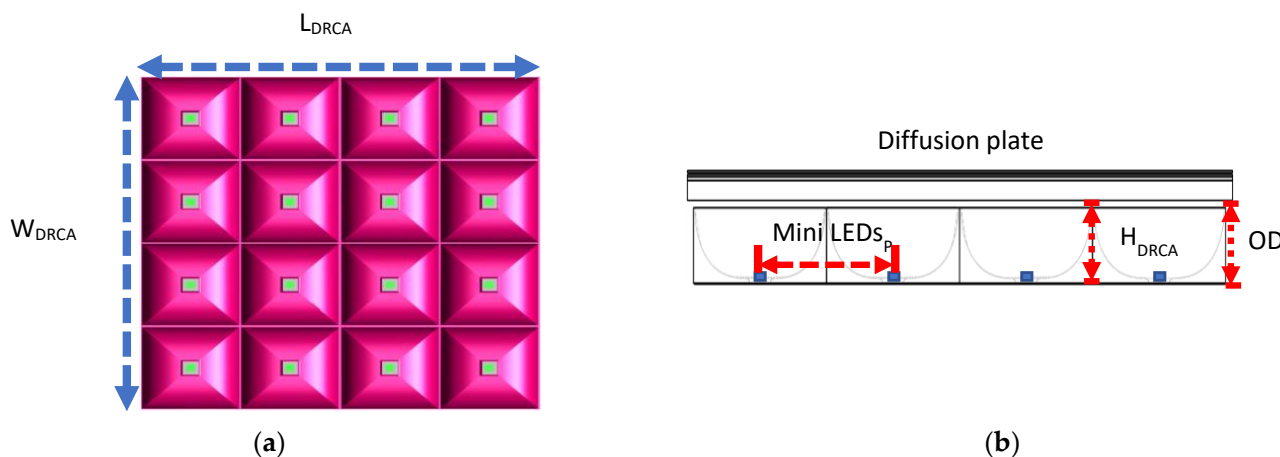


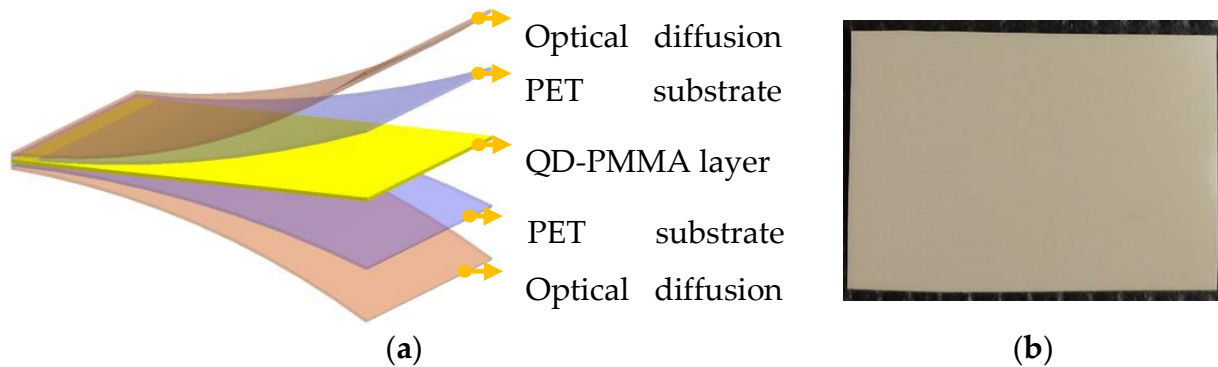
**Figure 5.** Schematic of the 3D structure of the  $4 \times 4$  diffuse reflection cavity matrix modules. (a) top view and (b) side view.

### 2.3. Fabrication of QD Film

Common QD film materials, such as green QDs ( $\lambda_g$ :  $\sim 530$  nm) and red QDs ( $\lambda_r$ :  $\sim 626$  nm) (both from Unique Materials Co. Ltd., Taichung city, Taiwan), were used. The quantum dots used in this article are red and green CdSe/ZnS. The particle size ranges of green and red quantum dots are 2.5–2.8 nm and 4.4–4.6 nm, respectively. The main reaction materials are cadmium oxide (CdO), zinc oxide (ZnO), silicon (Se) and Trioctylphosphine oxide (TOPO), lauric acid ( $C_{12}H_{24}O_2$ ), and n-hexane ( $C_6H_{14}$ ) material match reaction. Hexadecyl amine (HDA) was used to prevent the agglomeration reaction of QDs; methanol ( $CH_3OH$ ) was used to avoid agglomeration reaction, and argon (Ar) was used throughout the process to ensure inert atmosphere while growing the QDs.

The produced QDs were cured in Poly(methyl methacrylate) (PMMA); the weight ratio of quantum dots and PMMA glue is 20:1, and the weight percent concentration is 5 wt.%. The volume ratio of the red quantum-dots (QDs) and green QDs is 1:50.

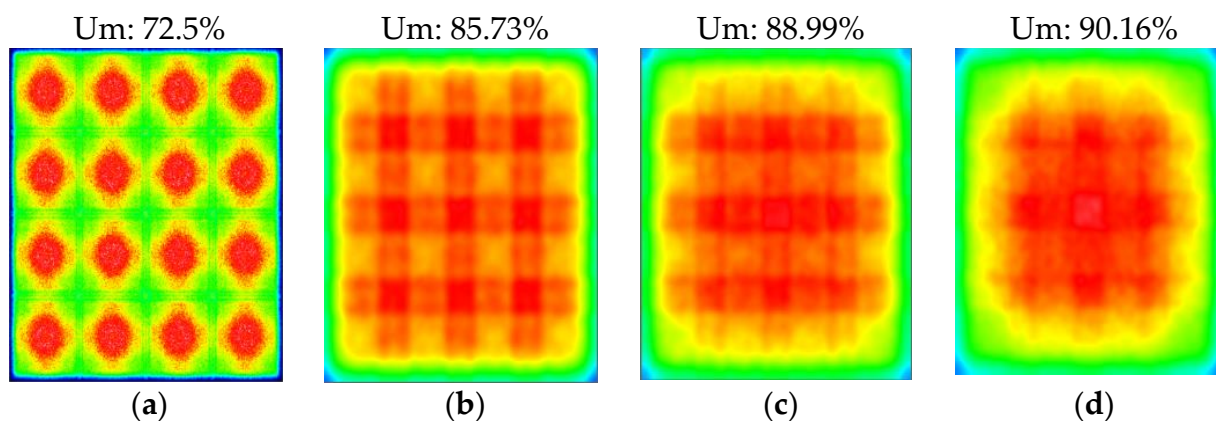
The QD-PMMA layer was coated between two PET film layers. Subsequently, the PET/QD-PMMA/PET film was laminated and cured using 365 nm ultraviolet radiation. Finally, a light diffusion layer was coated on the PET/QD-PMMA/PET film with a doctor blade coater. Figure 6 displays the structure.



**Figure 6.** Structure of QD color conversion film. (a) Various layers in structure and (b) actual sample.

#### 2.4. Simulation and Optimization of DRCA Structure

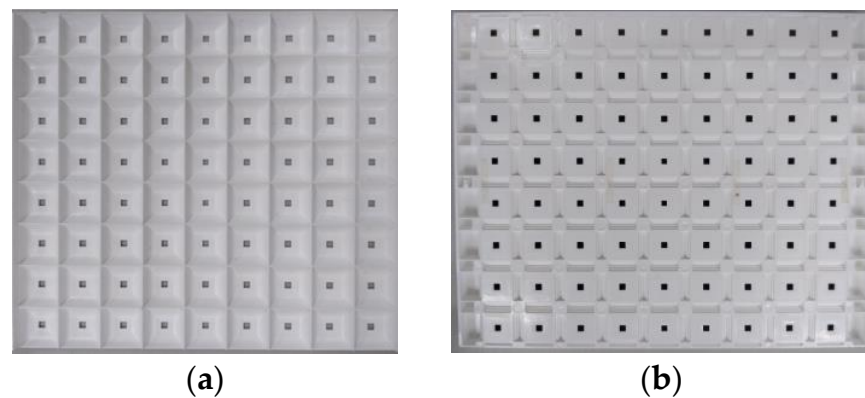
Figure 7 presents the simulation result. First, a simulation was performed to optimize the diffuse reflection cavity matrix. Subsequently, the diffuser and BEF were added in sequence, and their influence on the uniformity of the light was analyzed. The uniformity was calculated as  $\text{Min-luminance}/\text{Max-luminance} \times 100\%$ . Figure 7a reveals the optimized diffuse reflection cavity matrix. The mini-LED point light source was converted into a character with a wider light output area and uniformity of 72.5%. As indicated in Figure 7b, the diffuse reflection cavity matrix was projected onto an added diffuser to further expand the projection area and improve the uniformity to 85.73%. Figure 7c shows the addition of the first piece of the BEF. The simulation results indicated that adjusting the angle of light helped improve the uniformity to 88.99%. Finally, Figure 7d shows the addition of the first two pieces of BEF to adjust the concentrated light angle again and achieve uniformity of 90.16%.



**Figure 7.** Simulation and optimization results of mini-LEDs combined with the diffuse reflection cavity matrix. (a) Mini-LEDs combined with diffuse reflection cavity matrix, (b) additional diffuser, (c) additional diffuser and first BEF, and (d) additional diffuser and second BEF.

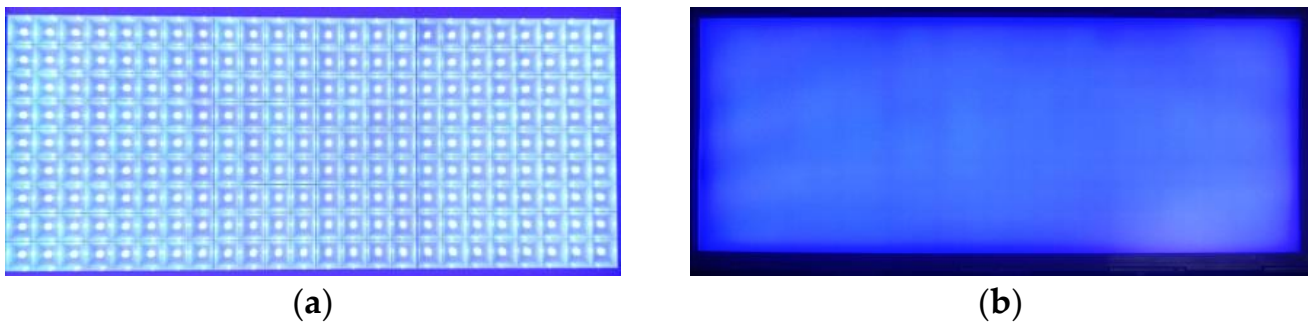
### 3. Results and Discussion

Figure 8 presents the front and back of the actual sample of the  $9 \times 8$  DRCA. The square transparent part in the figure is the diffuse reflection cavity, and the gray and black points in the center of the square are mini-LEDs.



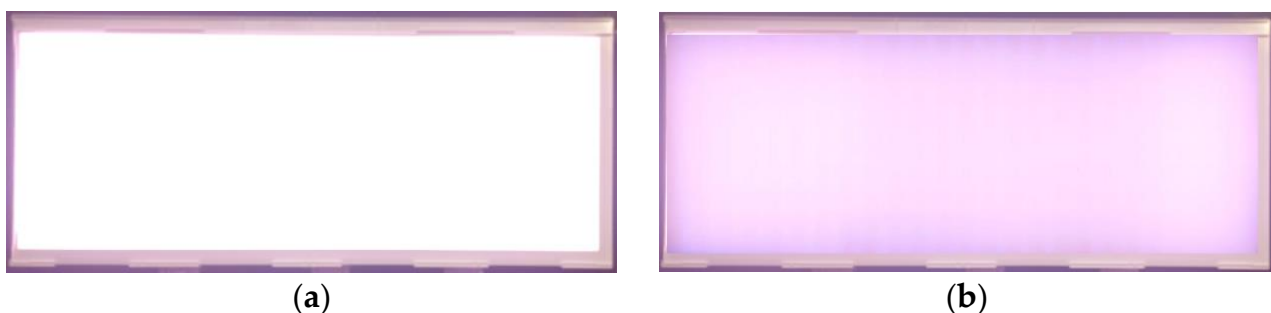
**Figure 8.** Actual sample of  $9 \times 8$  DRCA. (a) Front view and (b) back view of the diffuse reflection cavity.

Figure 9 depicts the actual sample of the 12.3-inch thin, large-area, high-brightness flat light source module. It comprises three groups of  $9 \times 8$  DRCA. The length, width, and height of the module are 292.8, 121, and 4.57 mm, respectively; the optical mixing distance is 6 mm, number of mini-LEDs is 216, and dynamic designable area comprises 216 zones.



**Figure 9.** Actual sample of a 12.3-inch thin blue large-area high-brightness flat light source module. (a) mini-LEDs combined with DRCA and (b) mini-LEDs combined with DRCA and diffuser.

Figure 10 shows the actual sample diagram of the 12.3-inch white light thin large-area high-brightness flat light source module. Figure 10a shows the light source module that comprises 216 wide-angle mini-LEDs combined with DRCA and QD color conversion film. Figure 10b shows mini-LEDs combined QD color conversion film without DRCA. The driving conditions are a forward voltage of 12 V and forward current of 1.65 A.



**Figure 10.** Actual sample diagram of 12.3-inch white light thin large-area high-brightness flat light source module, (a) mini-LEDs combined QD color conversion film with DRCA and (b) mini-LEDs combined QD color conversion film without DRCA.

Figure 11 presents the normalized light distribution curve obtained through an actual measurement. The black line indicates the light distribution curve of mini-LEDs combined with a DRCA. In this case, the central intensity value was 39.34%. The red line indicates

the light distribution curve of mini-LEDs combined with a DRCA and a diffuser. In this case, the central intensity value increased to 52.42%. The green line indicates the light distribution curve of mini-LEDs combined with a DRCA, a diffuser, and the first BEF. In this case, the central intensity value increased to 66.88%. The blue line indicates the light distribution curve of the mini-LEDs combined with a DRCA, a diffuser, and the second BEF. In this case, the central intensity value increased to 100%. These results indicate that for mini-LEDs combined with a DRCA as well as the first and the second BEF, the central light intensity can be increased by 1.7 and 2.54 times, respectively. The difference in light intensity between the two centers was 1.494 times.

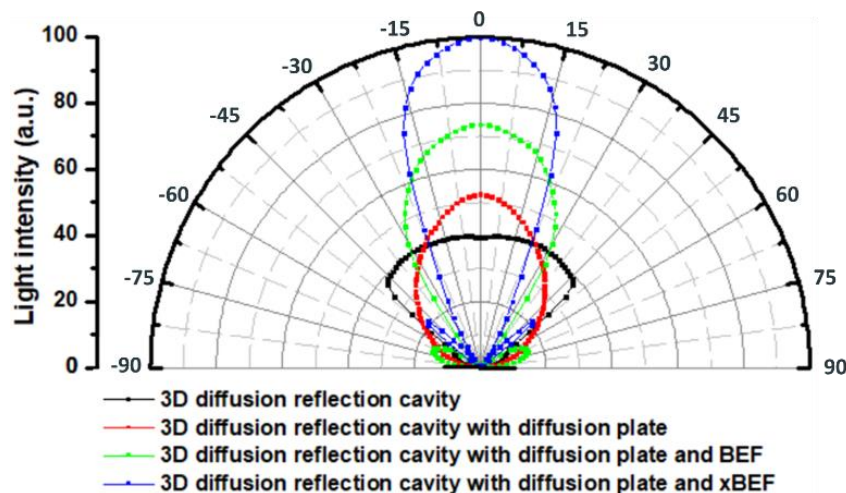


Figure 11. Light distribution curve of a 12.3-inch planar light source module with different structures.

The uniformity of the 12.3-inch white light thin large-area high-brightness planar light source module was measured using the nine-point measurement method commonly used in the industry. Figure 12 presents the measurement point distribution.

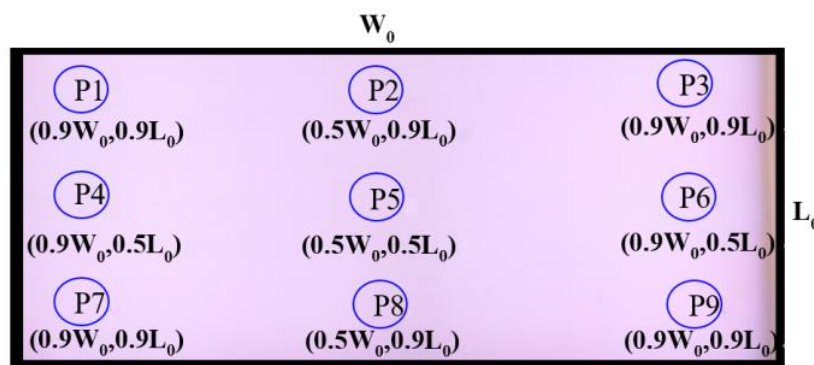


Figure 12. Brightness measurement points for the 12.3-inch white light thin large-area high-brightness flat light source module.

The uniformity was calculated as follows:

$$\text{Uniformity (\%)} = 100\% \times \frac{\text{minimum luminance (nits)}}{\text{maximum luminance (nits)}} \tag{4}$$

Table 2 lists the brightness value measured at nine measuring points and the uniformity value of the 12.3-inch mini-LEDs combined QD color conversion film with DRCAs of planar light source module. The driving conditions are a forward voltage of 12 V and forward current of 1.65 A. On average, the uniformity of the module was 87.58% when one BEF was added, and the brightness was 15,240 cd/m<sup>2</sup>. Furthermore, the uniformity of the module was 90.13% when two BEFs were added, and the average brightness

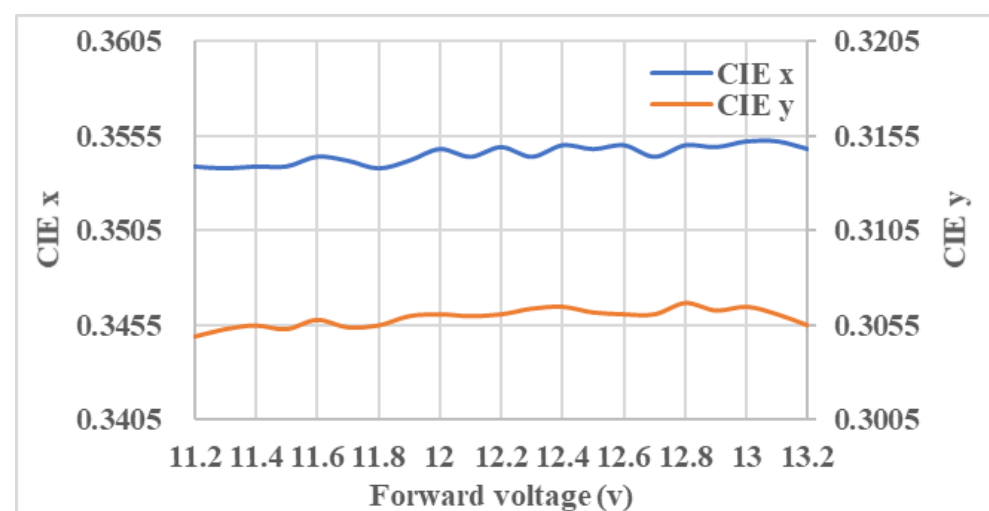


was 23,044  $\text{cd}/\text{m}^2$ . Therefore, the difference in average brightness between the two was 1.51 times. The average luminance value measured and the uniformity value of general mini-LED backlight that mini-LEDs combined QD color conversion film without DRCA is 19,370  $\text{cd}/\text{m}^2$  and 74.89%, respectively. Comparison of mini-LEDs backlight combined with DRCA and without DRCA shows that luminance is enhanced 1.18 times, and uniformity increases from 74.89% to 90.13%.

**Table 2.** Brightness and uniformity measured at nine points on the actual sample.

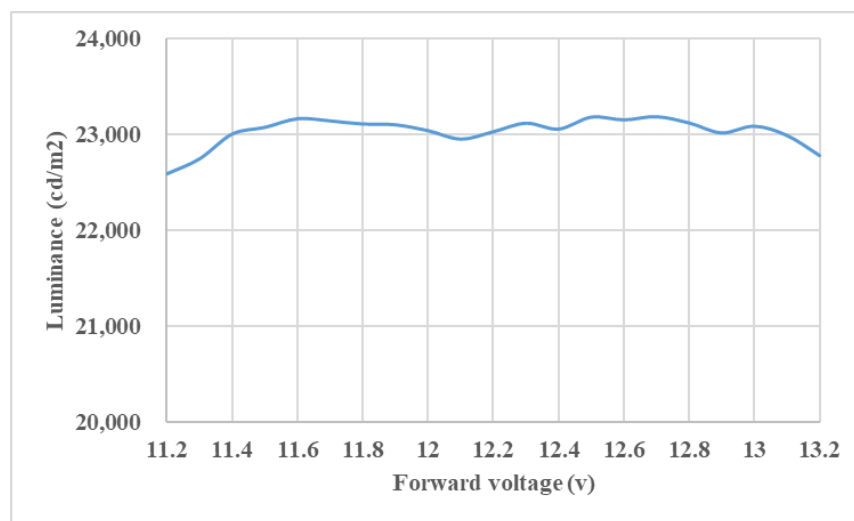
	1 BEF Luminance ( $\text{cd}/\text{m}^2$ )	2 BEF Luminance ( $\text{cd}/\text{m}^2$ )
P1	15,910	23,695
P2	14,220	21,785
P3	15,730	23,758
P4	16,218	24,025
P5	14,335	21,884
P6	15,276	23,255
P7	15,832	23,758
P8	14,205	21,655
P9	15,430	23,585
Average luminance/ CIE (x,y)	15,240/ CIE (x 0.3268,y 0.2845)	230,44/ CIE (x 0.3545,y 0.3059)
Uniformity (%)	87.58%	90.13%

Figure 13 displays the measured CIE color coordinates(x,y)-voltage of wide-angle mini-LEDs combined with a DRCA and QD film light source module. The forward voltage is increased from 11.2 V to 13.2 V, and the maximum variations in CIE x,y are 0.0014 and 0.0018, respectively.



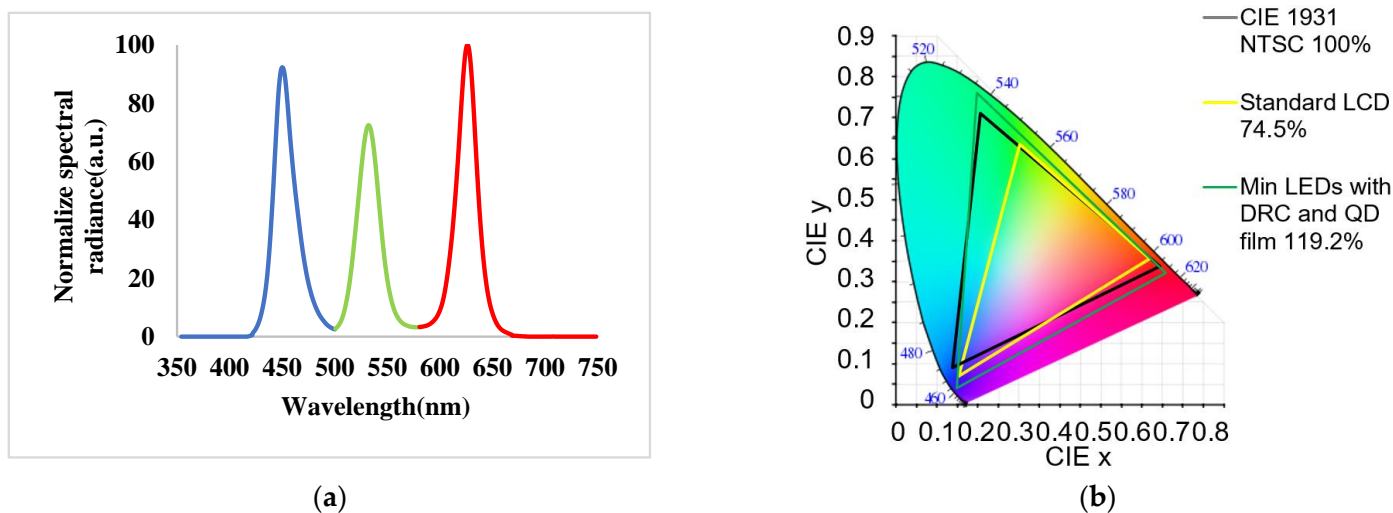
**Figure 13.** The measured CIE color coordinates (x,y)-voltage of wide-angle mini-LEDs combined with a DRCA and QD film light source module.

Figure 14 displays the measured luminance ( $\text{cd}/\text{m}^2$ )-voltage of wide-angle mini-LEDs combined with a DRCA and QD film light source module. The forward voltage is increased from 11.2 V to 13.2 V, the maximum variation percentage of luminance is 2.6%.



**Figure 14.** Displays the measured luminance ( $\text{cd}/\text{m}^2$ )–voltage of wide-angle mini-LEDs combined with a DRCA and QD film light source module.

Figure 15 displays the electroluminescence (EL) spectrum of wide-angle mini-LEDs combined with a DRCA and QD film light source module. In Figure 15a, the peak emission wavelengths are 450, 532, and 626 nm, and the FWHM is 20 nm. These results indicate that the mini-LEDs have the advantage of high color purity. According to the EL spectrum in the CIE 1931 color gamut coordinates, the mini-LEDs' NTSC reached 119.2%, as shown in Figure 15b, indicating their wide color gamut range.



**Figure 15.** (a) Normalized EL spectrum and (b) color gamut of mini-LEDs combined with a DRCA and QD film optical module.

#### 4. Conclusions

This study optimized the design of mini-LEDs combined with multiple 3D DRCA for application to thin, large-area, high-brightness, flat light source modules. A 12.3-inch white light thin, large-area, high-brightness planar light source module was used as a sample. The driving condition is a forward voltage of 12 V and a forward current of 1.65 A. At a mixing distance of 6 mm, the average luminance reached  $23,044 \text{ cd}/\text{m}^2$ , and NTSC was 119.2%. Comparison of mini-LEDs backlight combined with DRCA to that without DRCA shows that luminance is enhanced 1.18 times, and uniformity increases from 74.89% to 90.13%. The thin, large-area, high-brightness, high-uniformity, high-color-saturation planar light source module proposed in this study can be employed as the local dimming backlight in next-generation automotive displays.

**Author Contributions:** Z.T.Y., Y.H.C. and K.S.Y. designed the experiments. Y.H.C. analyzed the data. Z.T.Y. and K.H.L. discussed the results and contributed to the writing of the manuscript. All authors have read and agreed to the published version of the manuscript.

**Funding:** This work was financially/partially supported by the Advanced Institute of Manufacturing with High-Tech Innovations from the Featured Areas Research Center Program within the framework of the Higher Education Sprout Project by the Ministry of Education in Taiwan. This research was also supported by the Ministry of Science and Technology the Republic of China (Grant No. MOST 110-2218-E-002 -032 -MBK and 110-2221-E-194 -036) and EPOCH CHEMTRONICS Corp.

**Institutional Review Board Statement:** Not applicable.

**Informed Consent Statement:** Not applicable.

**Data Availability Statement:** Data sharing is not available.

**Conflicts of Interest:** The authors declare no conflict of interest.

## References

1. Huang, Y.; Hsiang, E.-L.; Deng, M.-Y.; Wu, S.-T. Mini-LEDs, Micro-LED and OLED displays: Present status and future perspectives. *Light Sci. Appl.* **2020**, *9*, 1–16. [[CrossRef](#)]
2. Chen, H.-W.; Lee, J.-H.; Lin, B.-Y.; Chen, S.; Wu, S.-T. Liquid crystal display and organic light-emitting diode display: Present status and future perspectives. *Light Sci. Appl.* **2017**, *7*, 17168. [[CrossRef](#)]
3. Zhou, X.; Tian, P.; Sher, C.-W.; Wu, J.; Liu, H.; Liu, R.; Kuo, H.-C. Growth, transfer printing and colour conversion techniques towards full-colour micro-LED display. *Prog. Quantum Electron.* **2020**, *71*, 100263. [[CrossRef](#)]
4. Lee, H.E.; Lee, D.; Lee, T.-I.; Shin, J.H.; Choi, G.-M.; Kim, C.; Lee, S.H.; Lee, J.H.; Kim, Y.H.; Kang, S.-M.; et al. Wireless powered wearable micro light-emitting diodes. *Nano Energy* **2018**, *55*, 454–462. [[CrossRef](#)]
5. Lo, Y.-K.; Wu, K.-H.; Pai, K.-J.; Chiu, H.-J. Design and Implementation of RGB LED Drivers for LCD Backlight Modules. *IEEE Trans. Ind. Electron.* **2009**, *56*, 4862–4871. [[CrossRef](#)]
6. Mei, W.; Zhang, Z.; Zhang, A.; Li, D.; Zhang, X.; Wang, H.; Chen, Z.; Li, Y.; Li, X.; Xu, X. High-resolution, full-color quantum dot light-emitting diode display fabricated via photolithography approach. *Nano Res.* **2020**, *13*, 2485–2491. [[CrossRef](#)]
7. Hames, B.C.; Mora-Seró, I.; Sánchez, R.S. Device performance and light characteristics stability of quantum-dot-based white-light-emitting diodes. *Nano Res.* **2017**, *11*, 1575–1588. [[CrossRef](#)]
8. Liu, Z.; Lin, C.-H.; Hyun, B.-R.; Sher, C.-W.; Lv, Z.; Luo, B.; Jiang, F.; Wu, T.; Ho, C.-H.; Kuo, H.-C.; et al. Micro-light-emitting diodes with quantum dots in display technology. *Light Sci. Appl.* **2020**, *9*, 1–23. [[CrossRef](#)]
9. Lee, X.-H.; Lin, C.-C.; Chang, Y.-Y.; Chen, H.-X.; Sun, C.-C. Power management of direct-view LED backlight for liquid crystal display. *Opt. Laser Technol.* **2013**, *46*, 142–144. [[CrossRef](#)]
10. Lee, T.-X.; Chen, B.-S. High Uniformity and Tolerance Design for Direct-Lit LED Backlight Illumination Using Lagrange Interpolation. *J. Disp. Technol.* **2016**, *12*, 1403–1410. [[CrossRef](#)]
11. Qin, Z. Luminance enhancement without sacrificing the viewing angle in a direct-lit backlight by addressing the angle-dependent characteristic of the prism film. *Displays* **2017**, *50*, 49–56. [[CrossRef](#)]
12. Kim, G.; Shih, Y.-C.; Shi, F. Optimal Design of Quantum Dot Color Conversion Film in LCD Backlighting. *IEEE J. Sel. Top. Quantum Electron.* **2017**, *23*, 011010. [[CrossRef](#)]
13. Chen, E.; Xie, H.; Huang, J.; Miu, H.; Shao, G.; Li, Y.; Guo, T.; Xu, S.; Ye, Y. Flexible/curved backlight module with quantum-dots microstructure array for liquid crystal displays. *Opt. Express* **2018**, *26*, 3466–3482. [[CrossRef](#)]
14. Zhou, X.; Qin, G.; Wang, L.; Chen, Z.; Xu, X.; Dong, Y.; Moheghi, A.; Yang, D.-K. Full color waveguide liquid crystal display. *Opt. Lett.* **2017**, *42*, 3706–3709. [[CrossRef](#)] [[PubMed](#)]
15. Zhang, X.; Qin, H.; Zhou, X.; Liu, M. Comparative evaluation of color reproduction ability and energy efficiency between different wide-color-gamut LED display approaches. *Optik* **2020**, *225*, 165894. [[CrossRef](#)]
16. Wu, T.; Sher, C.-W.; Lin, Y.; Lee, C.-F.; Liang, S.; Lu, Y.; Chen, S.-W.H.; Guo, W.; Kuo, H.-C.; Chen, Z. Mini-LED and Micro-LED: Promising Candidates for the Next Generation Display Technology. *Appl. Sci.* **2018**, *8*, 1557. [[CrossRef](#)]
17. Liao, H.; Zhao, M.; Zhou, Y.; Molokeev, M.S.; Liu, Q.; Zhang, Q.; Xia, Z. Polyhedron Transformation toward Stable Narrow-Band Green Phosphors for Wide-Color-Gamut Liquid Crystal Display. *Adv. Funct. Mater.* **2019**, *29*, 1901988. [[CrossRef](#)]
18. Oh, J.H.; Kang, H.; Ko, M.; Do, Y.R. Analysis of wide color gamut of green/red bilayered freestanding phosphor film-capped white LEDs for LCD backlight. *Opt. Express* **2015**, *23*, A791–A804. [[CrossRef](#)] [[PubMed](#)]
19. Shu, Y.; Lin, X.; Qin, H.; Hu, Z.; Jin, Y.; Peng, X. Quantum Dots for Display Applications. *Angew. Chem.-Int. Ed.* **2020**, *59*, 22312–22323. [[CrossRef](#)]
20. Kang, H.; Kim, S.; Oh, J.H.; Yoon, H.C.; Jo, J.-H.; Yang, H.; Do, Y.R. Color-by-Blue QD-Emissive LCD Enabled by Replacing RGB Color Filters with Narrow-Band GR InP/ZnSeS/ZnS QD Films. *Adv. Opt. Mater.* **2018**, *6*. [[CrossRef](#)]
21. Kim, H.-J.; Shin, M.-H.; Lee, J.-Y.; Kim, J.-H.; Kim, Y.-J. Realization of 95% of the Rec 2020 color gamut in a highly efficient LCD using a patterned quantum dot film. *Opt. Express* **2017**, *25*, 10724–10734. [[CrossRef](#)]

22. Ho, S.-J.; Chen, H.-S. Inverse  $\mu$ -photonic crystals enhanced the features of mini-sized quantum dot LEDs. *J. Mater. Chem. C* **2019**, *8*, 4309–4313. [[CrossRef](#)]
23. Huang, B.-L.; Guo, T.-L.; Xu, S.; Ye, Y.; Chen, E.-G.; Lin, Z.-X. Color Converting Film With Quantum-Dots for the Liquid Crystal Displays Based on Inkjet Printing. *IEEE Photonics J.* **2019**, *11*, 1–9. [[CrossRef](#)]
24. Moon, H.; Lee, C.; Lee, W.; Kim, J.; Chae, H. Stability of Quantum Dots, Quantum Dot Films, and Quantum Dot Light-Emitting Diodes for Display Applications. *Adv. Mater.* **2019**, *31*, e1804294. [[CrossRef](#)]
25. Lin, C.-L.; Chen, S.-C.; Deng, M.-Y.; Ho, Y.-H.; Lin, C.-A.; Tsai, C.-L.; Liao, W.-S.; Liu, C.-I.; Wu, C.-E.; Peng, J.-T. AM PWM Driving Circuit for Mini-LED Backlight in Liquid Crystal Displays. *IEEE J. Electron Devices Soc.* **2021**, *9*, 365–372. [[CrossRef](#)]
26. Tan, G.; Huang, Y.; Li, M.-C.; Lee, S.-L.; Wu, S.-T. High dynamic range liquid crystal displays with a mini-LED backlight. *Opt. Express* **2018**, *26*, 16572–16584. [[CrossRef](#)] [[PubMed](#)]
27. Huang, C.-H.; Chang, S.-H.; Liaw, B.-Y.; Liu, C.-Y.; Chou, C.-Y.; Zhou, J.-R.; Lin, C.-C.; Kuo, H.-C.; Song, L.; Feng, L.; et al. Research on a Novel GaN-based Converted Mini-LED Backlight Module via a Spectrum-Decouple System. *IEEE Access* **2020**, *8*, 138823–138833. [[CrossRef](#)]
28. Guo, W.; Chen, N.; Lu, H.; Su, C.; Lin, Y.; Chen, G.; Lu, Y.; Zheng, L.; Peng, Z.; Kuo, H.-C.; et al. The Impact of Luminous Properties of Red, Green, and Blue Mini-LEDs on the Color Gamut. *IEEE Trans. Electron Devices* **2019**, *66*, 2263–2268. [[CrossRef](#)]
29. Hsiang, E.-L.; Yang, Q.; He, Z.; Zou, J.; Wu, S.-T. Halo effect in high-dynamic-range mini-LED backlit LCDs. *Opt. Express* **2020**, *28*, 36822–36837. [[CrossRef](#)] [[PubMed](#)]
30. Hao, W.; Wang, F.; Guo, L.; Wang, J.; Guo, Z. Backlight Driving Circuit and Method, Backlight Module, Backlight Circuit and Display Device. U.S. Patent 10,726,774 B2, 28 July 2020.
31. Liu, C.-P. Display Module. U.S. Patent 2019/0243187 A1, 8 August 2019.
32. He, Z.; Yin, K.; Hsiang, E.-L.; Wu, S.-T. Volumetric light-shaping polymer-dispersed liquid crystal films for mini-LED backlights. *Liq. Cryst.* **2020**, *47*, 1458–1463. [[CrossRef](#)]
33. Chen, E.; Guo, J.; Jiang, Z.; Shen, Q.; Ye, Y.; Xu, S.; Sun, J.; Yan, Q.; Guo, T. Edge/direct-lit hybrid mini-LED backlight with U-grooved light guiding plates for local dimming. *Opt. Express* **2021**, *29*, 12179–12194. [[CrossRef](#)] [[PubMed](#)]
34. Ye, Z.-T.; Chen, C.-L.; Chen, L.-C.; Tien, C.-H.; Nguyen, H.-T.; Wang, H.-C. Hollow Light Guide Module Involving Mini Light-Emitting Diodes for Asymmetric Luminous Planar Illuminators. *Energies* **2019**, *12*, 2755. [[CrossRef](#)]
35. Ye, Z.-T.; Pai, Y.-M.; Chen, C.-H.; Kuo, H.-C.; Chen, L.-C. A Light Guide Plate That Uses Asymmetric Intensity Distribution of Mini-LEDs for the Planar Illuminator. *Crystals* **2019**, *9*, 141. [[CrossRef](#)]
36. Ohno, H. Design of a coaxial light guide producing a wide-angle light distribution. *Appl. Opt.* **2017**, *56*, 3977. [[CrossRef](#)]
37. Lu, B.; Wang, Y.; Hyun, B.-R.; Kuo, H.-C.; Liu, Z. Color Difference and Thermal Stability of Flexible Transparent InGaN/GaN Multiple Quantum Wells Mini-LED Arrays. *IEEE Electron Device Lett.* **2020**, *41*, 1040–1043. [[CrossRef](#)]
38. Lin, S.; Yu, J.; Cai, J.; Chen, E.; Xu, S.; Ye, Y.; Guo, T. Design of a freeform lens array based on an adjustable Cartesian candela distribution. *J. Mod. Opt.* **2019**, *66*, 2015–2024. [[CrossRef](#)]
39. Zhu, Z.-M.; Yuan, J.; Sun, X.; Peng, B.; Xu, X.; Liu, Q.-X. LED diffused transmission freeform surface design for uniform illumination. *J. Opt.* **2019**, *48*, 232–239. [[CrossRef](#)]
40. Huang, C.-H.; Kang, C.-Y.; Chang, S.-H.; Lin, C.-H.; Lin, C.-Y.; Wu, T.; Sher, C.-W.; Lin, C.-C.; Lee, P.-T.; Kuo, H.-C. Ultra-High Light Extraction Efficiency and Ultra-Thin Mini-LED Solution by Freeform Surface Chip Scale Package Array. *Crystals* **2019**, *9*, 202. [[CrossRef](#)]
41. Li, Z.-T.; Wu, J.-H.; Ren, Z.-Y.; Song, Y.-X.; Li, J.-S. Improving Ambient Contrast Ratio and Color Uniformity of Mini Full Color Light-Emitting Diodes Using an SiO<sub>2</sub>/Graphite Bilayered Packaging Structure. *J. Electron. Packag.* **2021**, *144*. [[CrossRef](#)]
42. Chen, L.-C.; Tien, C.-H.; Chen, D.-F.; Ye, Z.-T.; Kuo, H.-C. High-Uniformity Planar Mini-Chip-Scale Packaged LEDs with Quantum Dot Converter for White Light Source. *Nanoscale Res. Lett.* **2019**, *14*, 1–10. [[CrossRef](#)] [[PubMed](#)]
43. Park, Y.; Li, K.H.; Fu, W.Y.; Cheung, Y.F.; Choi, H.W. Packaging of InGaN stripe-shaped light-emitting diodes. *Appl. Opt.* **2018**, *57*, 2452–2458. [[CrossRef](#)] [[PubMed](#)]
44. Tang, B.; Miao, J.; Liu, Y.; Wan, H.; Li, N.; Zhou, S.; Gui, C. Enhanced Light Extraction of Flip-Chip Mini-LEDs with Prism-Structured Sidewall. *Nanomaterials* **2019**, *9*, 319. [[CrossRef](#)]
45. Zhu, Z.; Peng, B.; Yuan, J.; Xu, X. Design method of double freeform surface lens with diffuse reflection. *Light. Res. Technol.* **2019**, *52*, 247–256. [[CrossRef](#)]
46. Zhu, Z.-M.; Sun, X.; Peng, B. The Design of Diffuse Reflective Off-Axis Surface for Noncircular LED Arrays. *IEEE Photonics J.* **2016**, *9*, 1–10. [[CrossRef](#)]
47. Kikuchi, S.; Shibata, Y.; Ishinabe, T.; Fujikake, H. Thin mini-LED backlight using reflective mirror dots with high luminance uniformity for mobile LCDs. *Opt. Express* **2021**, *29*, 26724. [[CrossRef](#)]